Proceedings of the EuroGNC 2013, 2nd CEAS Specialist Conference
on Guidance, Navigation & Control, Delft University of Technology,
Delft, The Netherlands, April 10-12, 2013

Adaptive Control of Flutter Suppression of Wind Turbine Blade using Microtabs

Nailu Li[1] and Mark J. Balas[2], Pourya Nikoueeyan[3]

Abstract The control of aeroelastic response of a wind turbine blade is examined through theoretical and experimental studies. Motivated by the conventional trailing-edge flap control of flutter suppression, small-sized, low-cost, power-efficient microtabs are utilized as active flow control device, which is capable of affecting the flow over the blade to generate sufficient control force. The open-loop test of proposed model is presented by pole-zero analysis for flutter study and controllability detection. The designed Adaptive Controller responses well to the dynamics of the system via microtabs. The robustness and effectiveness of the controller are shown by good simulation performance within a wide range of aerodynamic loads in closed-loop experiments. The stability of the controller is proved theoretically by the given Adaptive Stability Theorem, which is also demonstrated by specified cases in details.

[1] Nailu Li

Phd student, Department of Electrical and Computer Engineering, University of Wyoming, Dept. 3295 1000 E. University Ave. Laramie, WY 82071, email: nli1@uwyo.edu

[2] Mark J. Balas

Head of Department and Professor, Department of Electrical and Computer Engineering, University of Wyoming, Dept. 3295 1000 E. University Ave. Laramie, WY 82071, email: mbalas@uwyo.edu

[3] Pourya Nikoueeyan

Graduate student, Department of Mechanical Engineering, University of Wyoming, Dept. 3295 1000 E. University Ave. Laramie, WY 82071, email: pnikouee@uwyo.edu

1 Introduction

Recent developments in wind turbine capability have resulted in flutter problem of large-sized blades, which harm the safety of wind turbine operation and reduce the efficiency of wind power generation. For the flow control, various actuators have been developed for the active suppression. Wing-flap on the trailing edge is a traditional and classic device for the past decades. Li adopted the flap for active flutter suppression of the flight[1]. A pitch-and-plunge aeroelastic system with flap is introduced by Zeng for flutter boundary expansion study[2]. And Kukreja also employed flap as actuator for nonlinear-system identification of aeroelastic systems[3]. In addition, another flow control with leading-edge and trailing-edge control was also focusing on two flap actuation devices on the aerofoil. Texas A&M University continued their study of aeroelastic system with globally stabilizing control achieved by using two control surfaces[4]. Multiple control surfaces are also utilized by Rao in addressing MIMO control problem[5].

However, for recent decades, active microtabs have been proposed as an effective and efficient device for active load control. The concepts involve that those small tabs can be positioned near trailing edge of an airfoil with large numbers and they can be deployed at certain rate perpendicular to the airfoil surface with a height, as to change the flow-field surround sufficiently to generate control force[6]. Several studies of those small-sized and low-cost devices have been carried on for flow control[7,8].

The concept of flow control using Microtabs is similar to the idea of gurney flaps, for which trailing edge flow development or so-called Kutta condition will vary and result in consequent changes in lift, and drag. Effect of these tabs on lift and moment coefficients of an airfoil has been shown to be as effective as conventional flaps[9] . For most of study, microtabs are utilized for experimental tests of lift and moment coefficients or open-loop control[10,11]. In this paper, Adaptive Control is adopted as the control algorithm in flutter suppression application.

The stability of designed controller is usually proved theoretically by Liapunov Theory[12]. However, in this paper, Adaptive Stability Theorem will not only be given and proved in theory, but also illustrated by proposed aeroelastic system with a wide range of aerodynamic loads. The robustness and effectiveness of Adaptive Controller are illustrated by good simulation results and numerical stability demonstration.

The rest of this paper is organized as following. In Sec. 2 involves development of system model and model analysis. Sec. 3 presents controller design and stability analysis. Sec. 4 shows simulation results of control strategy and demonstration of Stability Theorem with conclusions in Sec.5.

2 Model Development

2.1 *Aeroelastic model*

The blade model is a degree of freedom pitch and plunge system, with the actuator, microtab on the trailing edge, shown in Fig.1. The dynamic motion of this aeroelastic system are plunging and pitching, presented by plunge displacement h, down-forward and pitch angle θ, nose-up. The tabs installed on the trailing edge can be deployed approximately perpendicular to the airfoil surface to a height on the order of the boundary layer thickness as 2% of chord length. Lift enhancement and mitigation are achieved simply by deploying the tab on the pressure (bottom) and suction (upper) side of the airfoil respectively. When extending from pressure side of the airfoil near its trailing edge, it produces increase in lift coefficient while with suction side deployment, the lift coefficient decreases gradiently with the change of gurney-flap height g. The dynamics of actuator is also included for consideration.

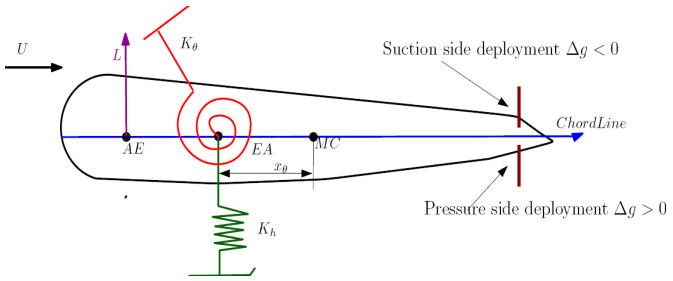

Fig.1 Aeroelastic system of two degree of freedom motion with Microtab on trailing-edge control surface.

Although the system is an aeroelastic system with actuator as mcriotab, effect of these tabs on lift and moment coefficients of an airfoil has been shown to be as effective as conventional flaps if the effect of aeroacoustic noise is neglected. Thus, the equations of motion for a wing section with two degree of freedom appear in the familiar form as[13]:

$$\begin{bmatrix} m & mx_\theta b \\ mx_\theta b & I_\theta \end{bmatrix}\begin{bmatrix} \ddot{h} \\ \ddot{\theta} \end{bmatrix}+\begin{bmatrix} C_h & 0 \\ 0 & C_\theta \end{bmatrix}\begin{bmatrix} \dot{h} \\ \dot{\theta} \end{bmatrix}+\begin{bmatrix} K_h & 0 \\ 0 & K_\theta \end{bmatrix}\begin{bmatrix} h \\ \theta \end{bmatrix}=\begin{bmatrix} -L \\ M \end{bmatrix} \quad (1)$$

where m is mass of blade section, I_θ is pitch moment of inertial about elastic axis, b is semichord, x_θ is distance from elastic axis to mass center, C_h, C_θ are plunge and pitch damping coefficients, and K_h, K_θ are plunge and pitch spring stiffness. The lift L and moment M are aerodynamic forces and moments, including trailing-edge gurney flap, defined as:

$$L = \rho U^2 b C_{l,\theta}(\theta + \frac{\dot{h}}{U} + (\frac{1}{2} - a)b\frac{\dot{\theta}}{U}) + \rho U^2 b C_{l,gf} g$$
$$M = \rho U^2 b^2 C_{m,\theta}(\theta + \frac{\dot{h}}{U} + (\frac{1}{2} - a)b\frac{\dot{\theta}}{U}) + \rho U^2 b^2 C_{m,gf} g \quad (2)$$

where ρ is air density, U is wind velocity, a is distance from midchord to elastic axis, and $C_{l,\theta}$,$C_{m,\theta}$, $C_{l,gf}$,$C_{m,gf}$ are lift and moment coefficients w.r.t angle of attack and gurney flap separately. For the control and stability analysis, the system needs to be transformed into state-space equation. Let the state variables be plunge displacement, pitch angle and derivatives of them and output y be pitch angle, we can obtain the aeroelastic model:

$$\dot{\mathbf{x}} = \begin{bmatrix} \mathbf{0}_{2\times 2} & I_{2\times 2} \\ -M_0^{-1}K_0 & -M_0^{-1}C_0 \end{bmatrix}\mathbf{x} + \begin{bmatrix} \mathbf{0}_{2\times 1} \\ M_0^{-1}R_0 \end{bmatrix}u$$
$$y = C\mathbf{x}, C = \begin{bmatrix} 0 & 1 & 0 & 0.1 \end{bmatrix} \quad (3)$$

where the control input u is the height of gurney flap g and the matrices M_0, K_0, C_0, R_0 are given in details in Appendix. The parameters of Eq. (1) and Eq. (2) are given in Table 1with all the constant parameters[2]. The lift/moment coefficients of gurney flap are derived from linear fittings of lift force/moment w.r.t gurney flap, which are computed by numerical simulation with commercial CFD code in FLUENT 6.3 software based on Reynolds-averaged Navier-Stokes equations. The fitted linear formulas are y=0.187x+0.0084 for lift force and y=-0.042x-2.3e-5 for the moment with unit of gurney flap as percent of chord length. Since the small intercept can be negligible, lift/moment coefficients are taken as 18.7 and -4.2 for non-dimensional gurney flap.

Table 1. Parameters of the aeroelastic model

Parameters	Value
ρ	1.225 kg/m^3
a	-0.6
b	0.135 m
K_h	2844.4 N/m
K_θ	2.82 N/m
C_h	27.43 kg/s
C_θ	0.18 kg m^2/s
m	12.387 kg
$C_{l,\theta}$	6.757
$C_{m,\theta}$	0

$C_{l,gf}$	18.7
$C_{m,gf}$	-4.2

2.1 *Model Analysis*

Since the aeroelastic system is a time-invariant system with 4 dimensions, the stability criterion can be decided by traditional method of eigenvalues-check. For the aeroelastic system, it's important to test the flutter speed, in order to identify flutter instability. In linear time-invariant system, the eigenvalues are equal to the poles of the system. So the figures of poles and zeros of open-loop system are plotted in the following figures according to various wind velocity from 5 m/s to 20 m/s.

Fig. 2 shows that for low wind velocity, the aeroelastic system can be stabilized by itself with all negative poles. As wind velocity increases, two negative poles move slightly toward the imaginary axis in Fig. 3. And when it reaches 13m/s in Fig. 4, there are two small poles located on right-hand side of the plane, which shows unstable for the system. For high wind velocity in Fig. 5, the instability can also be identified with two poles having real part around 5. Thus, we can conclude that the flutter speed of this aeroelastic system is 13 m/s. For all preflutter wind velocity, the open-loop system can stabilize itself without any control while the system are unstable with all postflutter wind velocity.

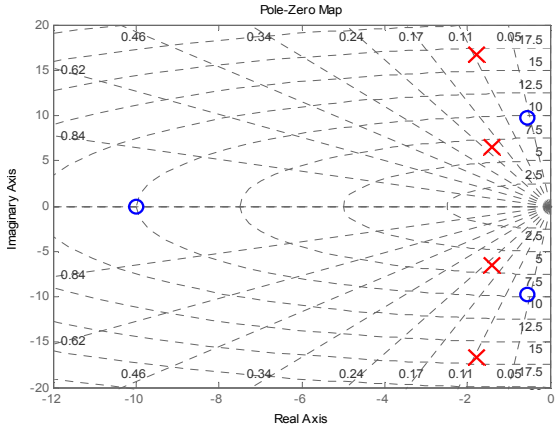

Fig. 2 Pole and zero map of open-loop system with U=5m/s

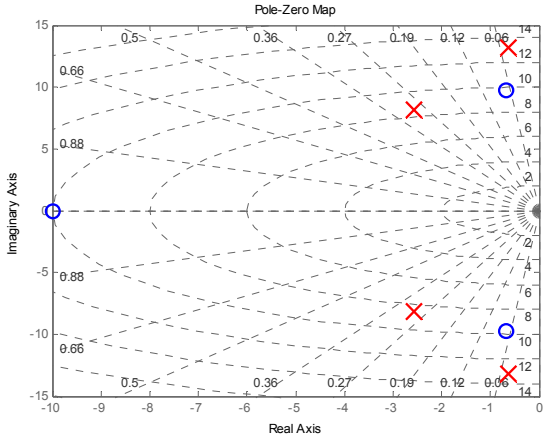

Fig. 3 Pole and zero map of open-loop system with U=12 m/s

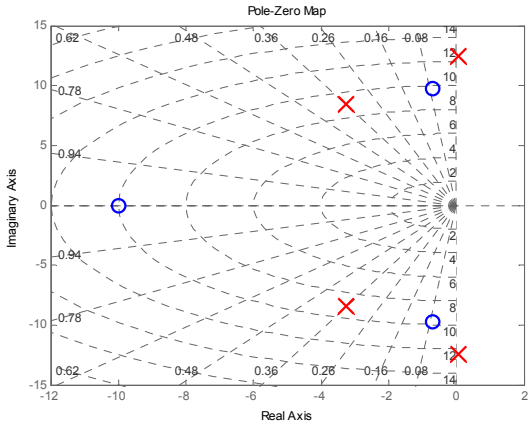

Fig. 4 Pole and zero map of open-loop system with U=13 m/s

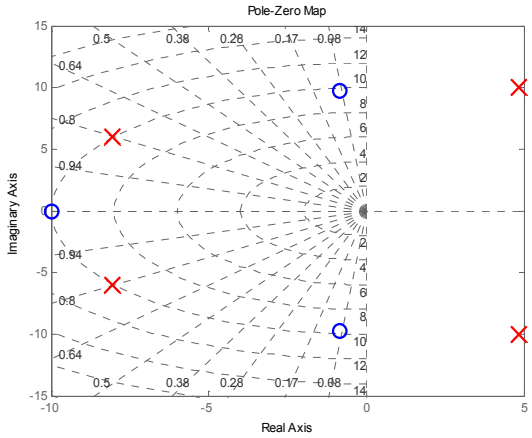

Fig. 5 Pole and zero map of open-loop system with U=20 m/s

It should also be noted that negative zeros are obtained for all the systems with a wide range of wind velocity, which indicates that the aeroelastic system with various static aerodynamic loads are applicable for Adaptive Control. The data of poles and zeros of the system on all conditions are given in Table 2.

Table 2. Eigenvalues and zeros of open-loop system

Wind Velocity	Eigenvalues (poles)	Zeros
5 m/s	-1.77 +16.72i, -1.77 -16.72i	-10, -0.55 + 9.75i
	-1.41 + 6.53i, -1.40 - 6.53i	-0.55 - 9.75i
12 m/s	-0.63 +13.19i, -0.63 -13.19i	-10, -0.68 + 9.74i
	-2.57 + 8.11i, -2.57 - 8.11i	-0.68 - 9.74i
13 m/s	0.05 +12.4i, 0.05 -12.4i	-10, -0.7 + 9.74i
	-3.25 + 8.46i, -3.25 - 8.456i	-0.7 - 9.74i

20 m/s	4.84 +10i, 4.84 -10i	-10, -0.83 + 9.7i
	-8 + 6i, -8 - 6i	-0.83 - 9.7i

3 Control Design and Stability Analysis

Since the output of the system is pitch angle, the value will vary with pitch command in different operation regions. It's assume that the wind turbine operates on Region III, where the rated wind power is kept by reducing pitch angle as wind velocity increases with rated speed 8m/s and cut-off speed 20m/s. For flutter suppression, out control goals includes two parts: stabilize the system, force plunge displacement and pitch angle asymptotically stable as time goes to infinity and achieve the desired pitch angle with relatively larger initial value.

The design of the Region III flutter suppression controller takes advantage of the adaptive disturbance tracking control approach. In this section, we develop the general adaptive control theory of PTS (periodic time-varying system). Although our plant is with all constant parameters, the time-varying version of Adaptive Control is still applicable to the time-invariant one.

The plant is assumed to be well modeled by the linear, time-varying, finite-dimensional system[14]:

$$\begin{cases} \dot{\mathbf{x}} = A(t)\mathbf{x} + B(t)\mathbf{u} + \Gamma(t)\mathbf{u}_D \\ \mathbf{y} = C(t)\mathbf{x} \\ \mathbf{x_0} = \mathbf{x}(0) \in R^{N_p} \\ \mathbf{u}_D = \Theta \mathbf{L} \phi_D \end{cases} \tag{4}$$

where y is the system output, pitch angle, A(t) is state matrix, B(t) is control input matrix, C(t) is output matrix and u_D is disturbance input: e.g. a step input, which is composed by basic function $\phi_D(t) \equiv 1, t_0 = 1$ with unknown amplitude matrices (Θ,L).

Based on the idea of control objectives along with rejection of disturbance, we define the output error as $e_y = y - y^*$. Our goal is to make output error converge to 0 asymptotically as time goes to infinite. Then this control goal can be achieved by an Adaptive Control Law as:

$$\begin{cases} \mathbf{u} = \mathbf{G}_e \mathbf{e}_y + \mathbf{G}_D \phi_D \\ \dot{\mathbf{G}}_e = -\mathbf{e}_y \mathbf{e}_y^T \gamma_e \\ \dot{\mathbf{G}}_D = -\mathbf{e}_y \phi_D^T \gamma_D \end{cases} \tag{5}$$

where G_e and G_D are adaptive gains, which are specified in Eq. (5) with arbitrary positive definite matrices γ_e, γ_D . Here, since the output y and disturbance $\phi_D(t)$ are one dimensional, γ_e, γ_D are positive scalars.

In order to confirm the stability of the designed controller in Eq. (4), the Adaptive Stability Theorem is given as:

Definition 1. $\exists$ positive constants $p_{\min}, p_{\max}, q_{\min}$

$$\ni \begin{cases} p_{\min}\|x\|^2 \le V(t,x) = x^T P(t) x \le p_{\max}\|x\|^2 \\ q_{\min}\|x\|^2 \le x^T Q(t) x \end{cases}$$

where P(t) and Q(t) matrices satisfy Kalman-Yacubovic Lemma with feedback system (A_c(t),B(t),C(t)):

$$\begin{cases} \dot{P}(t) + A_C{}^T(t)P(t) + P(t)A_C(t) = -Q(t) < 0, P(t) > 0 \\ P(t)B(t) = C^T(t) \end{cases}$$

Theorem 1. *if*
1) (A(t), B(t),C(t)) satisfy Definition 1;
2) (A(t),B(t),C(t))is bounded (as is the case when time-invariant);
3) $\phi_D(t)$ *is bounded;*
4) $\exists G_D{}^* \ni BG_D{}^* + \Gamma\Theta L = 0$ *;*
Then Adaptive Control $u = Ge_y + G_D\phi_D$ *with adaptive gains in Eq. (5) produces* $e_y \xrightarrow[t\to\infty]{} 0$ *with bounded adaptive gains(*G_e*,* G_D*) .*

Proof. We firstly take the system trajectory as idea trajectory (x_*, y_*, u_*) with deviations ($\Delta x, \Delta y, \Delta u$) as follows[15]:

$$\begin{cases} \Delta\mathbf{x} \equiv \mathbf{x} - \mathbf{x}_* \\ \Delta\mathbf{u} \equiv \mathbf{u} - \mathbf{u}_* = \mathbf{u} \\ \Delta\mathbf{y} \equiv \mathbf{y} - \mathbf{y}_* = \mathbf{e}_y \end{cases} \tag{6}$$

And the idea trajectory is given as[14]:

$$\begin{cases} \dot{\mathbf{x}}_* = A\mathbf{x}_* + B\mathbf{u}_* + \Gamma\mathbf{u}_D \\ \mathbf{y}_* = C\mathbf{x}_* \\ \mathbf{x}_* = S_1\mathbf{z}_D \\ \mathbf{u}_* = S_2\mathbf{z}_D \end{cases} \tag{7}$$

where z_D is disturbance state as $\mathbf{z}_D = \mathbf{L}\phi_D$, The ideal trajectories, which are for theorical analysis, will not be needed by actual controller.

Based on Eq. (6) and Eq. (7), the deviation of control input u can be obtained as:

$$\Delta \mathbf{u} = \Delta \mathbf{G}_e \mathbf{e}_y + \mathbf{G}_e^* \mathbf{e}_y + \Delta \mathbf{G}_D \phi_D \tag{8}$$

where the idea adaptive gain $G_D^*=S_2L$, G_e^* is the desired feedback gain, and the deviations are defined as $\Delta G_e=G_e-G_e^*$,$\Delta G_D=G_D-G_D^*$.

Then we have the deviation of feedback system from idea trajectory:

$$\begin{cases} \Delta \dot{\mathbf{x}} = A_C \Delta \mathbf{x} + Bw \\ \Delta \mathbf{y} = C \Delta \mathbf{x} = \mathbf{e}_y \\ A_C \equiv A + BG_e^* C \end{cases} \tag{9}$$

Now, we define the lyapynov candidate function of the system as;

$$V(t,x) = \Delta x^T P(t) \Delta x \tag{10}$$

Then, we can check the derivative of V(t,x) as follows:

$$\begin{aligned} \dot{V}(t,\Delta x) &\equiv \frac{\partial}{\partial t} V + \nabla V \Delta \dot{x} \\ &= \Delta x^T \dot{P}(t) \Delta x + 2\Delta x^T P(t) \Delta \dot{x} \\ &= \Delta x^T (\dot{P}(t) + A_C{}^T(t) P(t) + P(t) A_C(t)) \Delta x + 2\Delta x^T \underbrace{P(t)B(t)}_{C^T(t)} w \\ &= -\Delta x^T Q(t) \Delta x + 2\langle y, w \rangle \end{aligned}$$

It's also defined that $V(\Delta G) \equiv tr(\Delta G \gamma^{-1} \Delta G^T) \Rightarrow \dot{V}(\Delta G) = -2\langle y, w \rangle$

Therefore,

$$\begin{aligned} &V(t,\Delta x,\Delta G) \equiv V(t,\Delta x) + V(\Delta G) \\ &\Rightarrow \dot{V}(t,\Delta x,\Delta G) = \dot{V}(t,\Delta x) + \dot{V}(\Delta G) \\ &\qquad = -\Delta x^T Q(t) \Delta x + 2\langle y, w \rangle - 2\langle y, w \rangle \\ &\qquad = -\Delta x^T Q(t) \Delta x \le -q_{\min} \left\| \Delta x \right\|^2 \le 0 \end{aligned}$$

$\therefore$ all trajectories $(\Delta x, \Delta G)$ are bounded.

Also

$W(x) \equiv q_{\min} \left\| \Delta x \right\|^2$ satisfies:

$\dot{W}(x) = q_{\min}\Delta x^T \Delta \dot{x} = q_{\min}\Delta x^T (A_C(t)\Delta x + B(t)w)$,which is bounded when ϕ_D is bounded, and $(A(t), B(t), C(t))$ are bounded. Applying Barbalat's Lemma to $W(\Delta x)$, we'll have $W(\Delta x) \xrightarrow[t\to\infty]{} 0$,which leads to $\Delta x \xrightarrow[t\to\infty]{} 0$ as desired. Thus $e_y = C\Delta x \xrightarrow[t\to\infty]{} 0$.

4 Simulation and Results

Since the wind turbine blade operates on Region Ⅲ, it's assumed that the desired pitch angle is 10 deg with initial value 15 deg. With the rated speed of 8m/s, the experiments are complemented at 10m/s, 13m/s, 15m/s and 20m/s separately. For consideration of practical condition of microtab, gurney flap g is saturated to vary between $\pm$2% of chord length. Moreover, the input disturbance is not considered in this paper. In order to have an insight into the control behavior of the designed Adaptive Controller, the simulation results of state responses of both open-loop and closed-loop systems are shown as follows with initial condition (h(0),θ(t))=(0,15 deg) .

4.1 *Simulations of State Responses*

For lower wind velocity, the open-loop system is stable as shown in Fig. 6. However, without any control, the pitch angle only converges to some constant rather then the desired 10 deg, which reveals that the system still needs to be adapted to the reach the control aim even at preflutter speed. At the same time, the pitch angle response reaches 10 deg with initial value 15 deg as expected. And the response of plunge displacement h in closed-loop system is also well stabilized with smaller overshoot in a estimated settling time of 4 second compared with the one in open-loop system. It should be noted that the steady state of closed-loop h response is a small non-zero constant instead of zero, due to the fact that our desired pitch angle is no longer 0, which will make the plunge displacement balance at a position rather than horizontal line.

Fig.7 shows that open-loop responses tend to be unstable with a high frequency when the system achieves the flutter speed U=13 m/s while the Adaptive Control still performs well in suppressing pitching and plunging, and attaining desired pitch angle. In addition, h response is stable at a little further position away from horizontal line.

As postflutter speed is gained, the response of open-loop system totally blow up after around 8 second simulation time shown in Fig.8. In contrast, Adaptive Controller does a good job in forcing pitch angle reach 10 deg and stabilizing the system.

Fig. 6 State responses of open-loop and closed-loop systems at U=10 m/s

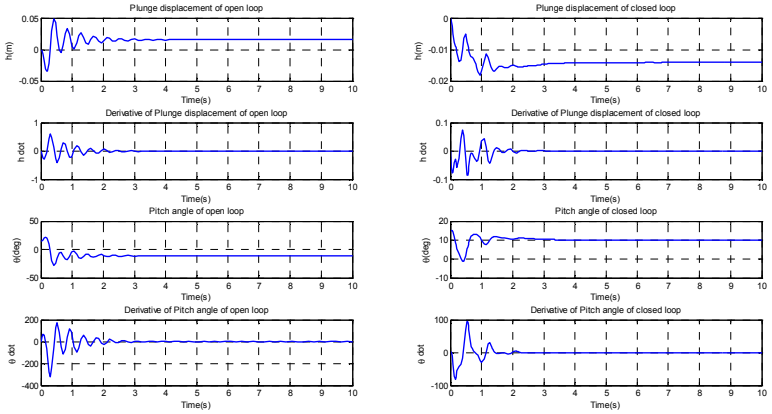

Fig. 7 State responses of open-loop and closed-loop systems at U=13 m/s

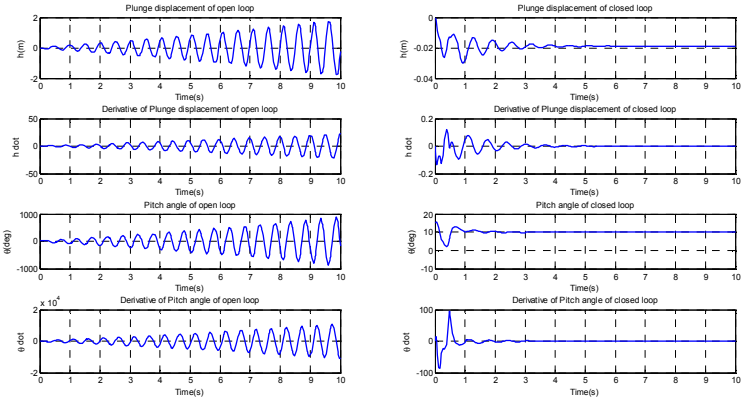

With high wind velocity 20 m/s in Fig. 9, the state responses of open-loop system blow up in a more extreme way while the Adaptive Controller can stabilize the system with small plunge displacement. Thus, we can conclude that the simulation results are in good agreement with the outcomes of model analysis in Table 2.

Fig. 8 State responses of open-loop and closed-loop systems at U=15 m/s

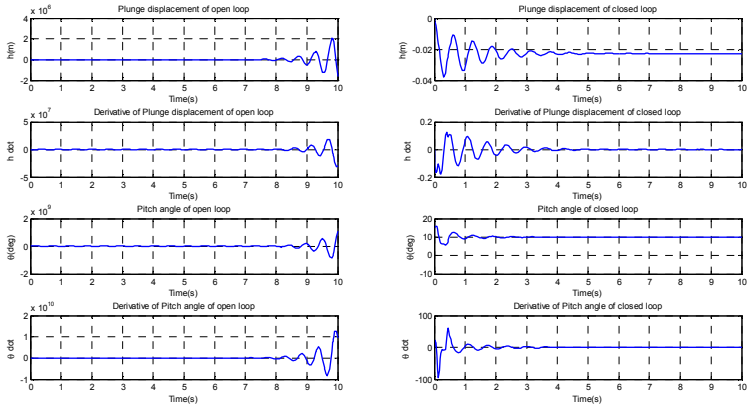

Fig. 9 State responses of open-loop and closed-loop systems at U=20 m/s

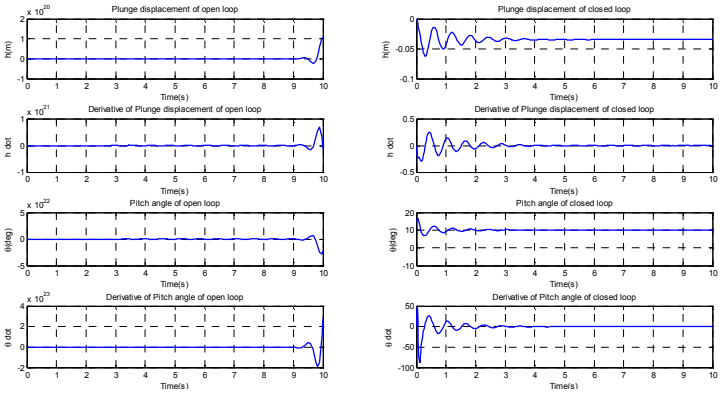

4.2 *Simulations of Control Surface*

In this part, to demonstrate control ability of microtab, several simulation tests are implemented with diverse wind velocity, showing the responses as plunge displacement, pitch angle and gurney flap separately in Fig. 10 to Fig. 13. It's noted that the unit of gurney flap is non-dimensional.

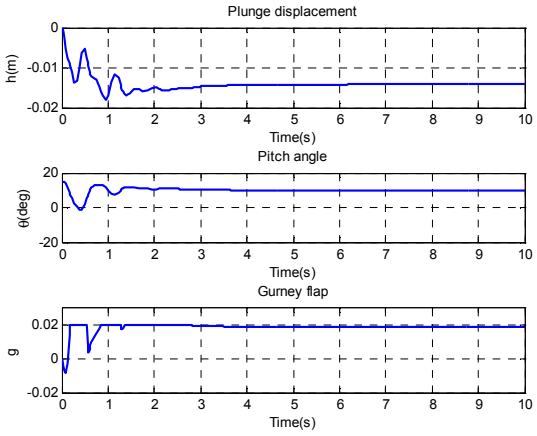

Fig. 10 Closed-loop plunge displacement, pitch angle and control input at U=10 m/s<U_F

Fig. 10 shows that the closed-loop system can response well to the saturated gurney flap g within the range of $\pm 2\%$. For this preflutter velocity, the desired pitch angle can be attained in a settling time, 4 seconds.

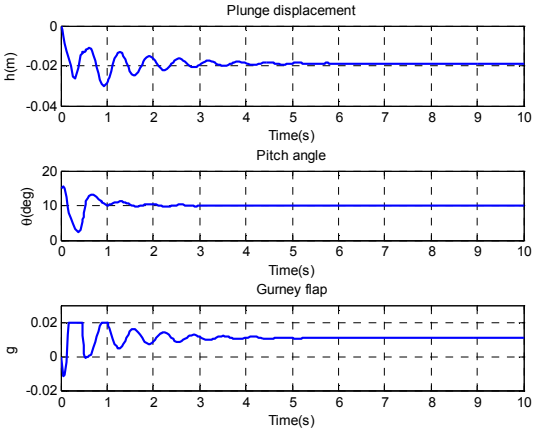

Fig. 11 Closed-loop plunge displacement, pitch angle and control input at U=13 m/s=U_F

When it comes to the flutter speed, the saturated control input still performs well in stabilizing all state responses within a relatively longer settling time as around 5 seconds, due to the fact that the divergent open-loop system at flutter speed takes more time to be stabilized than the convergent one at preflutter speed.

For postflutter speed in Fig.12 and Fig.13, the smaller g is needed to reach the control aim with increasing wind velocity because the larger gain is obtained by the Adaptive Controller at high velocity with a shorter settling time.

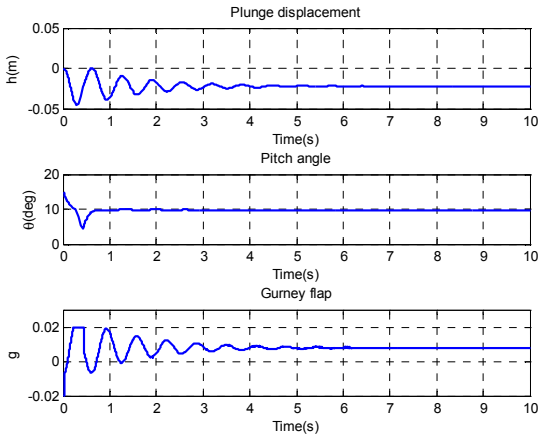

Fig. 12 Closed-loop plunge displacement, pitch angle and control input at U=15 m/s>U_F

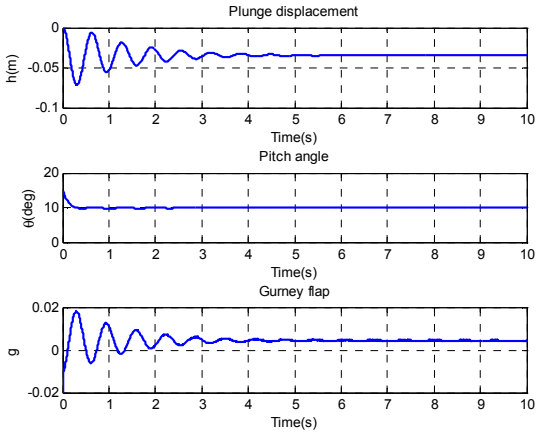

Fig. 13 Closed-loop plunge displacement, pitch angle and control input at U=20 m/s>U_F

Therefore, Adaptive Control can still perform well in reaching a non-zero desired output with nonzero initial value using saturated gurney flap for diverse wind velocity. Note that non-zero reference tracking for Adaptive Control is because of the nonzero plunge displacement. But h response can converge to a very small constant with small overshoot in a relative short settling time, estimated 4 second, which can be treated as effective plunging suppression.

4.2 *Demonstration of Adaptive Stability Theorem*

Stability of the given Adaptive Controller is firstly shown by good simulations above. In this part, the proposed stability theorem is also demonstrated numerically by our feedback aeroelastic system. Since our plant is time invariant

system at each wind velocity, the K-Y equations in Definition 1 will be solved for the demonstration with constant (A_c,B,C).

The first case is the aeroelastic system with U=10 m/s. Our goal is to find positive definite matrices P and Q with positive p_{min}, p_{max} and q_{min} . The solved P and Q for this case are shown as follows:

$$P = \begin{bmatrix} 13.4546 & 0.8859 & 0.0142 & 0.0015 \\ 0.8859 & 1.1087 & 0.0291 & 0.0060 \\ 0.0142 & 0.0291 & 0.1426 & 0.0151 \\ 0.0015 & 0.0060 & 0.0151 & 0.0019 \end{bmatrix},$$

$$Q = \begin{bmatrix} 2.7174 & -2.5377 & 0.1697 & 0.0180 \\ -2.5377 & 10.3474 & 0.1827 & 0.0193 \\ 0.1697 & 0.1827 & 0.3408 & 0.0259 \\ 0.0180 & 0.0193 & 0.0259 & 0.0988 \end{bmatrix}$$

Thus, we can obtain that p_{min}=2.82e-4, p_{max}=13.54, q_{min}=0.096, which are all positive. We can conclude that the feasible P and Q matrices have been found.

The solutions of the system with the rest of wind velocity cases are illustrated in Table 3, where solved P and Q are positive definite with all positive p_{min}, p_{max} and q_{min} for every single case. The solutions illustrate the stability of closed-loop system, showing good agreement with simulation results. So, the Adaptive Stability Theorem is successfully demonstrated for all wind velocity.

Table 3. Solutions of Stability Theorem for different wind velocity cases

Wind Velocity(m/s)	p_{min}	p_{max}	q_{min}
13	1.689e-4	13.74	0.0972
15	1.274e-4	12.5	0.0976
20	7.2e-5	8.33	0.0981

5 Conclusion

A pitch and plunge aeroelastic system is established for the study in demonstrating the aeroelastic control capabilities of Microtabs and for exploring Adaptive Control techniques. Model analysis has been completed with the flutter speed study and controllability checking. The gurney flap is saturated as the control input, showing the control capability of Microtabs. The Adaptive Controller is designed to adapt to unsteady dynamics of postflutter system and to achieve the control objective. Closed-loop test is then implemented to successfully reveal Microtabs' ability in flutter suppression. The good application of Microtabs with a wide range of wind velocity is illustrated by simulation results and numerical demonstration of Adaptive Stability Theorem.

Appendix

The matrices in Eq. (3) can be given as:

$$M_0 = \begin{pmatrix} m & mx_\theta b \\ mx_\theta b & I_\theta \end{pmatrix}, K_0 = \begin{pmatrix} K_h & \rho U^2 b C_{l,\theta} \\ 0 & K_\theta - \rho U^2 b^2 C_{m,\theta} \end{pmatrix},$$

$$C_0 = \begin{pmatrix} C_h + \rho U b C_{l,\theta} & \rho U b^2 C_{l,\theta}(\frac{1}{2} - a) \\ -\rho U b^2 C_{m,\theta} & C_\theta - \rho U b^3 C_{m,\theta}(\frac{1}{2} - a) \end{pmatrix}, R_0 = \begin{pmatrix} \rho U^2 b C_{l,gf} \\ \rho U^2 b^2 C_{m,gf} \end{pmatrix}.$$

Acknowledgments

The authors acknowledge support for this work through grant DESC0001261 from the Department of Energy monitored by Timothy J. Fitzsimmons. Additional support was provided through a gift from BP Alternative Energy North America Inc.

References

1. Li G., Dong C., and Hou Y., "Active Flutter Suppression using Robust Adaptive Switching Control," in *Proc. of 48th IEEE Conf. on Decision and Control 28th Chinese Control Conf.*, Shanghai, China, 2009.
2. Zeng J., Callafon D. R. and Brenner M., "Adaptive Feedback Control Algorithm for Flutter Boudary Expansion", *AIAA Atmospheric Flight Mechanics conference*, Chicago, IIIinois, 2009.

3. Kukreja S. L., "Non-Linear System Identification for Aeroelastic Systems with Application to Experimental Data", *AIAA Guidance, Navigation and Control Conference and Exhibit*, Honolulu,Hawaii, 2008.
4. Platanitis G. and Strganac T. W., "Control of a Nonlinear Wing Section Using Leading- and Trailing-Edge Surface," *Journal of Guidance, Control, and Dynamics*, vol. 27, No.1, January-February 2004.
5. Rao V. M., Beha A., and Marzocca P., "Hierarchical Adaptive Controller for a Nonlinear Aeroelastic Wind Section with Multiple Control Surfaces," in *Proc. of 44th IEEE Conf. on Decision and Control, and the European Control Conf.*, Seville, Spain, 2005.
6. Bieniawski S. and Kroo I. M., "The impact of Coherent Turbulence on Wind Turbine Aeroelastic Response and Its Simulation", *AIAA Structures, Structural Dynamics, and Material Conf.*, Norfolk, Virginia, 2003.
7. Kelley N. D., et. al, "Flutter Suppression Using Micro-Trailing Edge Effectors", *Wind Power 2005 Conf.*, NREL/CP-500-38074, August 2005.
8. McCoy, T. J. and Griffin D. A., "Active Control of Rotor Geometry and Aerodynamics: Retractable Blades and Advanced Devices", *AWEA WINDPOWER 2007 conference,* Los Angeles, CA., June 4-6, 2007.
9. Kuik, T.K. Barlas and Van G.A.M., "Review of state of the art in smart rotor control research for wind turbines",1, s.l. : Elsevier, January 2010, Progress in Aerospace Sciences, Vol. 46, pp. 1-27.
10. Maughmer D. M. and Bramesfeld G., "Experimental Investigation of Gurney Flaps," *Journal of Aircraft*, vol. 45, No.6, November-December 2008.
11. Tang D. and Dowell H. E., "Aerodynamic Loading for an Airfoil with an Oscillating Gurney Flap," *Journal of Aircraft*, vol. 44, No.4, July-August 2007.
12. Reddy K. K., Chen J. and Behal A., "Multi-Input/Multi-Output Adaptive Output Feedback Control Design for Aeroelastic Vibration Suppression," *Journal of Guidance, Control, and Dynamics*, vol. 30, No.4, July-August 2007.
13. Ko J., Kurdila A. J., and Strganac, T.W., "Nonlinear Control of a Prototypical Wing Section with Torsional Nonlinearity," *Journal of Guidance, Control and Dynamics*, Vol.20, No.6, Nov.-Dec. 1997, pp.1181-1189.
14. Balas M., and Li Q., "Adaptive Disturbance Tracking Control for Large Horizontal Axis Wind Turbines in Variable Speed Region Ⅱ Operation," *Computer Engineering*, Jan., 2010, pp. 2010-2010.
15. Balas J. M. and Li N. "Adaptive Control of Flow over a Wind Turbine Blade", AIAA GNC/AFM/MST/ASC, Minneapolis, Minnesota, 2012.